Electronic Supplementary Information

Charge Transport Modulation in Pseudorotaxane 1D Stacks of Acene and Azaacene Derivatives

1. General Methods

Reagents for synthesis were, if not otherwise specified, purchased from Aldrich, Fluka or Acros. Commercial chemicals and solvents were used as received. Column chromatography was carried out using Silica gel 60 (40-60 μm) from Scharlab. Analytical thin layer chromatography (TLC) was done using aluminum sheets (20x20 cm) pre-coated with silica gel RP-18W 60 F254 from Merck. UV-active compounds were detected with a UV-lamp from CAMAG at wavelength λ = 254 or 366 nm.

NMR spectra were recorded on Bruker Avance 400 and 500 spectrometers at 298 K using partially deuterated solvents as internal standards. Coupling constants (*J*) are denoted in Hz and chemical shifts (*δ*) in ppm. Multiplicities are denoted as follows: s = singlet, d = doublet, t = triplet, m = multiplet, br = broad.

Matrix Assisted Laser Desorption Ionization (coupled to a Time-Of-Flight analyzer) experiments (MALDI-TOF) were recorded on Bruker REFLEX spectrometer in Polymat by Dr. Antonio Veloso.

Absorption spectra were recorded in KBr pellets under N_2 atmosphere on a Cary 5000 spectrometer.

Fluorescence spectra were registered on a *LS55* Perkin-Elmer Fluorescence spectrometer.

2. Synthesis

Macrocycle **1** was synthesized according to reported procedures.[1] Phenazine **2** is commercially available and while its oxidation to obtain phenazine **3** and **4** were synthesized according to reported procedures with 30% H_2O_2 and acetic acid.[2] Phenazine **5** was obtained following a variation of the classic Wohl-Aue method.[3]

Mono-*N*-oxy 2,7-Dimetoxyphenazine (6) and di-*N*-oxy 2,7 - dimetoxyphenazine (7)

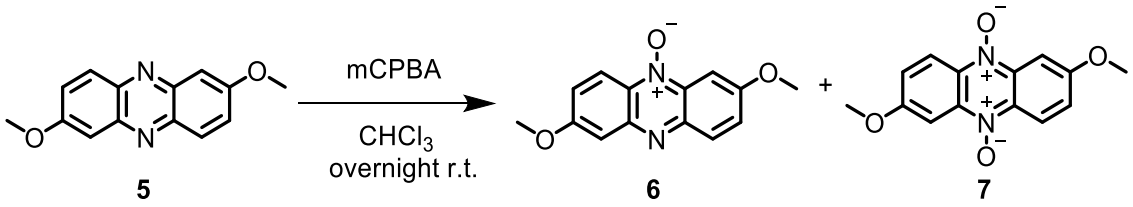

5 **6** **7**

mCPBA at 70 % (265 mg, 1.07 mmol) was added to a solution of phenazine **5** (300 mg, 1.24 mmol) in $CHCl_3$ (30 mL). The solution was stirred overnight at room temperature under N_2. The orange solution formed was washed with a saturated Na_2CO_3 solution and H_2O. The organic phase was dried over Na_2SO_4, filtered and finally the solvent was removed under reduced pressure. The mixture obtained was purified by column chromatography (CH_2Cl_2/AcOEt, 9.4:0.6). **6** and **7** were obtained and recrystallized from EtOH giving yellow and red needles respectively (171 mg, 62 % and 48 mg, 16 %).

6:

m.p. 245-246 ºC. **^{1}H NMR** (400 MHz, $CDCl_3$): δ = 8.59 (d, *J* = 9.5 Hz, 1H), 8.00 (d, *J* = 9.4 Hz, 1H), 7.89 (d, *J* = 2.4, 1H), 7.46 (dd, *J* = 9.4, 2.5 Hz, 1H), 7.36-7.43 (m, 2H), 4.03 (s, 1H), 3.99 (s, 1H) ppm. **^{13}C NMR** (126 MHz, $CDCl_3$) δ = 161.1, 160.9, 145.3, 142.7, 134.8, 131.1, 130.9, 126.4, 125.1, 120.1, 106.0, 95.7, 56.4, 56.0 ppm. **EM (MALDI-TOF)** (m/z): calculated for $[M]^+$ $C_{14}H_{12}N_2O_3$: 256.084, found: 256.586.

7:

m.p. 240-242 ºC. **^{1}H NMR** (400 MHz, $CDCl_3$): δ = 8.64 (d, *J* = 9.7 Hz, 2H), 7.96 (d, *J* = 1.4 Hz, 2H), 7.48 (dd, *J* = 1.4, 9.7 Hz, 2H), 4.06 (s, 6H) ppm. **^{13}C NMR** (126 MHz, $CDCl_3$) δ = 161.88, 136.13, 132.54, 125.75, 121.59, 97.21, 56.61 ppm. **EM (MALDI-TOF)** (m/z): calculated for $[M]^+$ $C_{14}H_{12}N_2O_4$: 272.080, found: 272.628.

Polycrystalline powders of the pseudorotaxanes were prepared mixing equimolecular solutions of both, macrocycle **1** and phenazines **2-7**. The solutions were mixed and stirred under nitrogen until a homogenous solution was achieved. Following this, EtOH was added to the solution until it became turbid and then the solid was allowed to precipitate. The solid was collected by centrifugation, washed with EtOH and finally with pentane.

Table S1. Yields and decomposition points (d.p.) of pseudorotaxanes **2@1**-**7@1** formation

Pseudorotaxane	**2@1**	**3@1**	**4@1**	**5@1**	**6@1**	**7@1**
Yield [%]	90	93	48	53	78	71
d.p. [ºC] (no melting)	340	270	305	335	330	320

3. NMR spectra for compounds 6-7

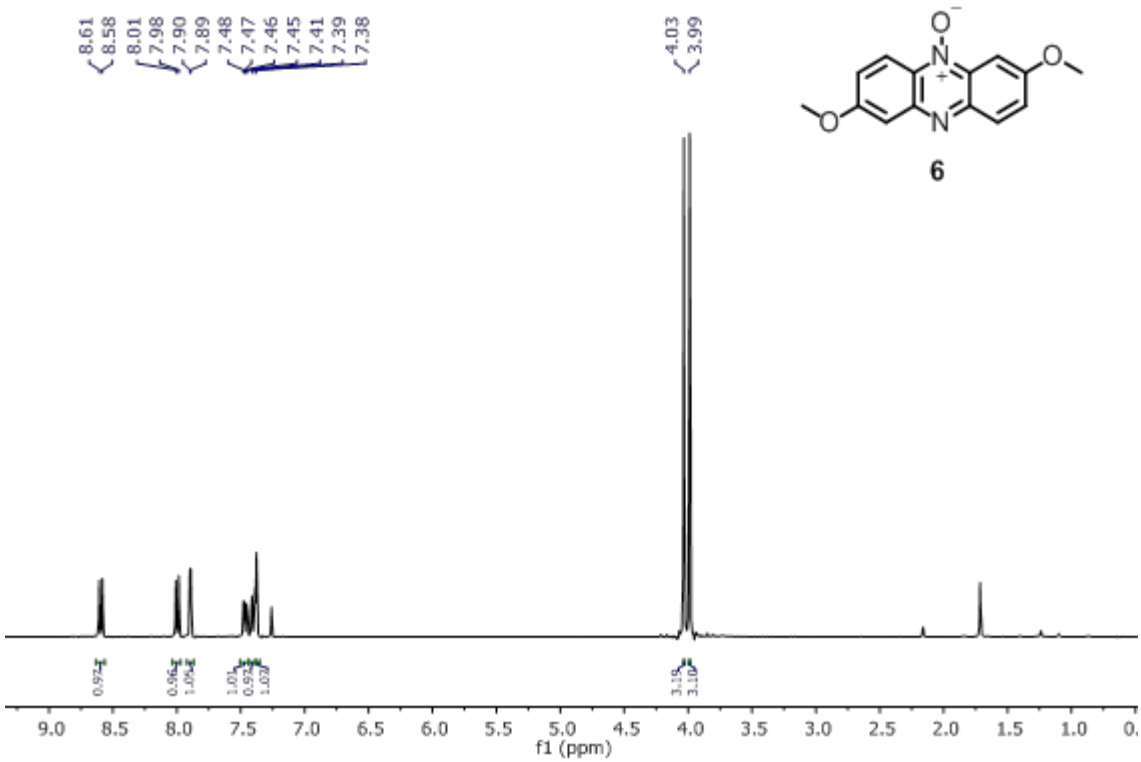

Figure S1: ^{1}HNMR spectrum of phenazine **6** (400 MHz, $CDCl_3$, 298 K).

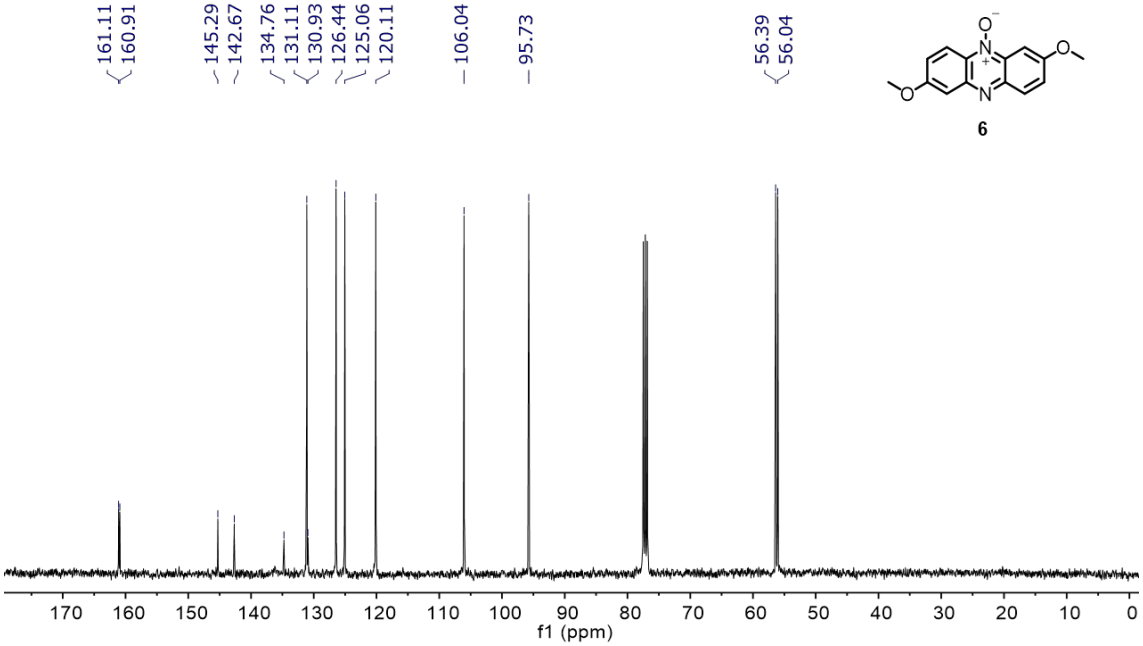

Figure S2: ^{1}HNMR spectrum of phenazine **6** (126 MHz, $CDCl_3$, 298 K).

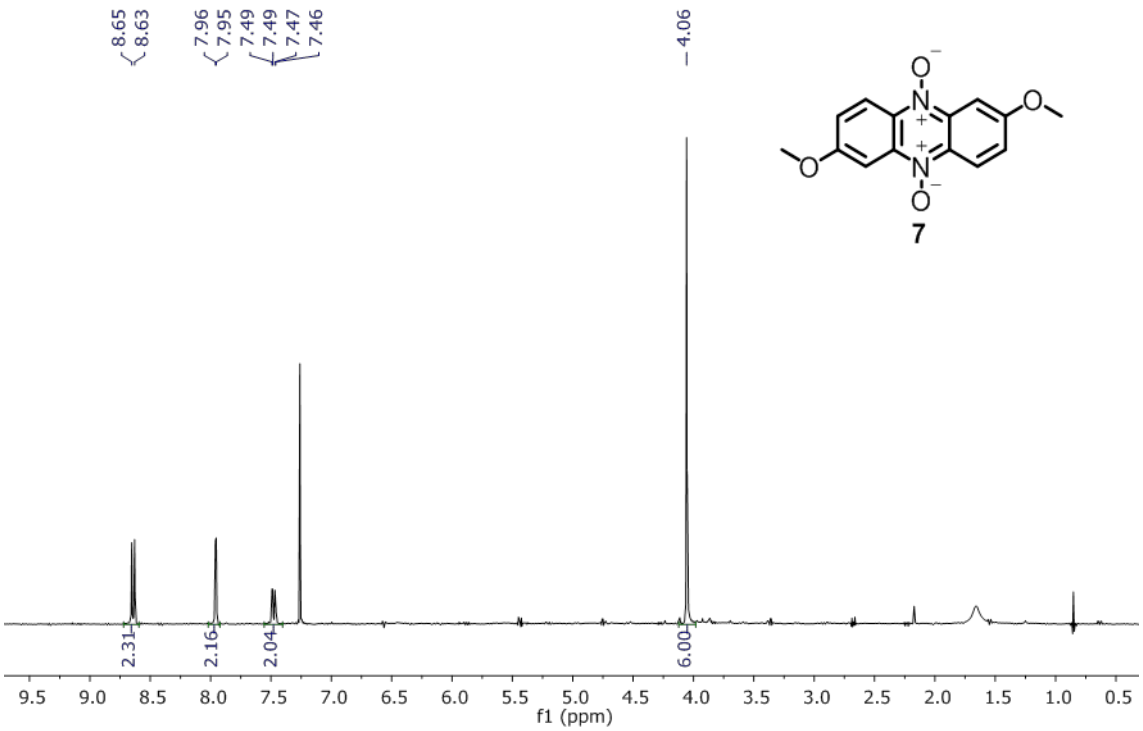

Figure S3: ^{1}HNMR spectrum of phenazine **7** (400 MHz, $CDCl_3$, 298 K).

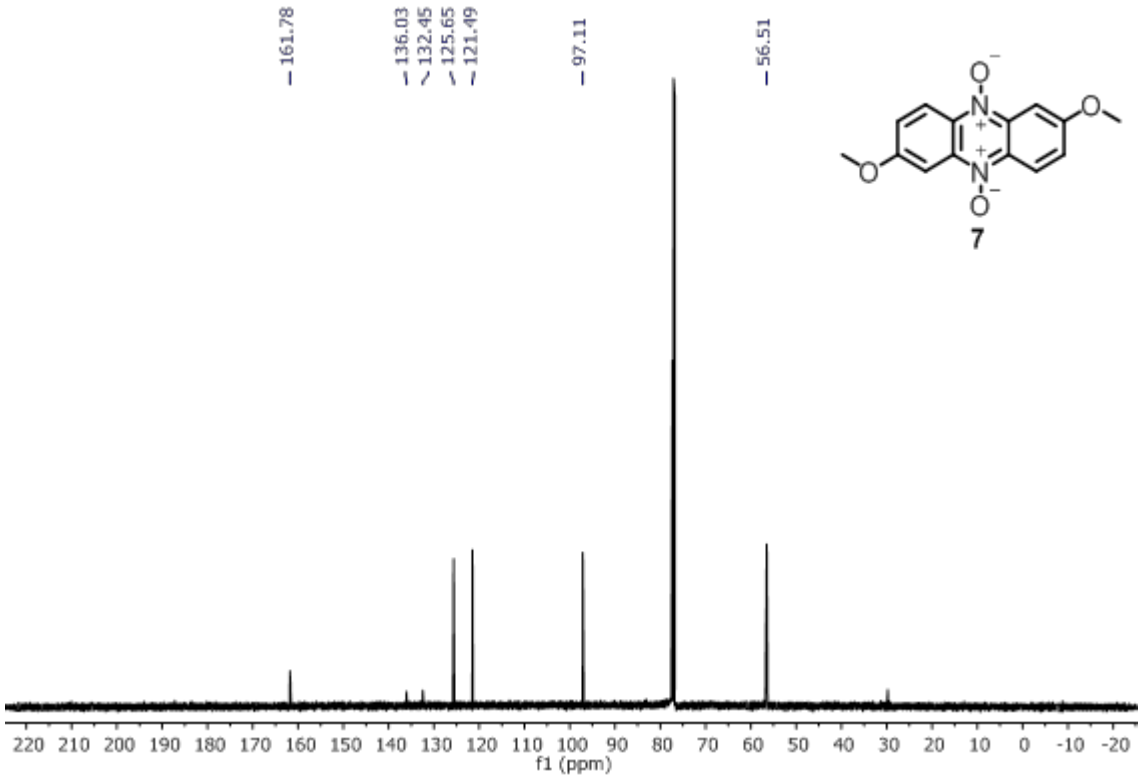

Figure S4: ^{1}HNMR spectrum of phenazine **7** (126 MHz, $CDCl_3$, 298 K).

4. Single Crystal X-Ray Diffraction

X-ray diffraction experiments were performed by the X-ray diffraction unit of General Services SG-Iker (UPV/EHU) by Dr. Leire San Felices. Intensity data were collected on an Agilent Technologies Super-Nova diffractometer, which was equipped with monochromated Cu kα radiation (λ= 1.54184 A) and Atlas CCD detector. Measurement was carried out at 100(2) K with the help of an Oxford Cryostream 700 PLUS temperature device. Data frames were processed (united cell determination, analytical absorption correction with face indexing, intensity data integration and correction for Lorentz and polarization effects) using the Crysalis software package. The structure was solved using Olex2 and refined by full-matrix least-squares with SHELXL-97. Final geometrical calculations were carried out with Mercury and PLATON as integrated in WinGX.

Crystallographic data for **1** (CCDC-1850666), **2@1** (CCDC-1850667), **3@1** (CCDC-1850668), **4@1** (CCDC-1850669), **5@1** (CCDC-1850670), **6@1** (CCDC-1850671), **7@1** (CCDC-1850672), are deposited in the Cambridge Crystallographic Data Centre.

The conditions of crystallization are reported in table S2. Macrocycle **1** was and pseudorotaxanes **2@1**-**7@1** were crystallized in inert conditions by low diffusion of a solvent into a solution of the corresponding compound. In the case of pseudorotaxanes **2@1**-**7@1** were used (1:1) stoichiometric ratios of phenazines and macrocycle **1.**

Table S2. Conditions of crystallization of macrocycle **1** and pseudorotaxanes **2@1**-**7@1** by liquid-liquid diffusion. TCE = 1,1,2,2-tetrachloroethane.

Compound	Solvent difused	Solvent	Concentration (mM)
1	EtOH	TCE	3.18
2@1	Hexane	TCE	3.18
3@1	EtOH	TCE	3.18
4@1	EtOH	TCE	3.18
5@1	Hexane	TCE	3.18
6@1	-----	$CHCl_3$	10.0
7@1	EtOH	TCE	6.18

Macrocycle **1** (monoclinic *P 1 2_1/c 1*) crystallizes in a chair-like conformation with a cavity between the anthracene units of 7.21 Å (Figure 2), in which two ethanol molecules are trapped (not shown). Macrocycle **1** organizes forming chains where one pyridyl ring stacks in an antiparallel fashion with another pyridyl ring to an adjacent macrocycle. The centroid to plane distances between pyridyl rings alternate 3.61 and 3.53 Å values along the chain (Figure 2 shows averaged values). The pyridyls from one chain are stacked to the anthracene rings of a parallel chain at centroid to plane distances that alternate 3.59 and 3.45 Å values (Figure 2 shows averaged values). Such little distortions are due to the different arrangement of the ethanol molecules (not shown) in the cavity.

The macrocycle in **2@1** (triclinic *P-1*) adopts a flattened chair conformation (180º) and shows that the four NH residues of the macrocycle **1** form bifurcated intramolecular hydrogen bonds (Figure 2). The N atoms of the central pyrazine ring of phenazine **2** engage in hydrogen bonds with the macrocycles' amides ($dNH\cdots N_{phen}$ = 2.54 and 2.36 Å) with an additional contribution of the intramacrocycle hydrogen bonds between the amides and the pyridinic N ($dNH\cdots N_{pyr}$ = 2.45 and 2.46 Å). Also, phenazine **2** is π-stacked between the two anthracene units of macrocycle **1** in an almost co-facial (eclipsed) arrangement with an equal centroid to plane distance of 3.38 Å in the same range as the graphitic interlayer distance. Phenazine **2** and the two anthracene units are essentially flat, but **2** is not parallel with respect to the anthracene units (the

planes are twisted by 6°). Pseudorotaxane **2@1** piles up in columns, so the anthracene rings of the adjacent complexes sit on one another through π-stacking at a distance of 3.51 Å.

The macrocycle in pseudorotaxane **3@1** (orthorhombic *P n a 2₁*) adopts an almost flat (174°) chair conformation (Figure 2). Both the N-oxide and the sp^2 N of the phenazine are bound to the macrocycle by bifurcated hydrogen bonds (dNH···O_{phen} = 2.14 and 2.21 Å; dNH···N_{phen} = 2.42 and 2.34 Å) with a contribution from the pyridine ring of the macrocycle (dNH···N_{pyr} = 2.41 and 2.44 Å; 2.41 and 2.41 Å, respectively from the *N*-Oxide and the N side). Phenazine **3** lies twisted within the cavity and sits at a distance of 3.42 Å and 3.49 Å from the anthracenes. The anthracene units and phenazine **3** are placed perfectly parallel and staggered along the longitudinal axis of the phenazine and the anthracenes. **3@1** piles up in columns arranged in a herringbone pattern, where the intracolumnar distances between the pseudorotaxane units is 3.57 Å.

The crystal structure of pseudorotaxane **4@1** (triclinic *P-1*) showed two conformational isomers of the same pseudorotaxane with minor structural differences (Figure 2). The macrocycle of pseudorotaxane **4@1** adopts a bent chair conformation with two different angles (142º and 150º). The NH residues of macrocycle **1** are also formed by bifurcated hydrogen bonds with the phenazine di-*N*-oxide **4** (dNH···O_{phen} = 2.20, 2.15, 2.14, 2.13 Å) and with the pyridine of the macrocycle (dNH···N_{pyr} = 2.41, 2.39, 2.40, and 2.38 Å). Phenazine di-*N*-oxide **4** is sandwiched between the two anthracenes of macrocycle **1** with different distances to the anthracene units (3.42 Å and 3.41 Å). The structure shows alternate columns of the conformational isomers of **4@1**, where the interplanar distances between pseudorotaxanes units are 3.56 Å.

Pseudorotaxane **5@1** (triclinic *P1*) crystallizes in a similar fashion as **2@1** (Figure 3), where the macrocycle also adopts a chair conformation (130°). Dimethoxyphenazine **5** is encapsulated within the cavity by means of hydrogen bonds between the amides of the macrocycle and the N atoms of the phenazine (d NH···N_{phen}= 2.45 and 2.34 Å) and with the pyridinic N (dNH···N_{pyr} = 2.36 and

2.35 Å). The hydrogen bonds are shorter in comparison to **2@1**, which is consistent with the electron-donating methoxy substituents that increase the hydrogen bond basicity of the electron-accepting nitrogen in the phenazine. In addition, phenazine **5** is π-stacked within the cavity with a distance of 3.54 Å from the phenazine to the different anthracenes and is slightly displaced from a cofacial arrangement because of the methoxy substituents. The aromatic framework of phenazine **5** in the complex is essentially flat, while the anthracene moieties appear to be slightly distorted from planarity (12°), also as an effect of the underlying methoxy groups of phenazine **5**. Pseudorotaxane **5@1** also piles up in slightly slipped 1D columns, in which the anthracene rings of adjacent complexes are π-stacked one on top of the other at a 3.45 Å distance.

6@1 crystals suitable for X-ray diffraction were particularly difficult to obtain and less refined structures were obtained from the diffracting crystals. Nevertheless, from the crystal structure, it was possible to confirm the encapsulation and packing in agreement with the rest of the crystal structures. An almost flat chair conformation (165^{o}) was observed for the macrocycle in pseudorotaxane **6@1** (triclinic *P-1*) (Figure 3). Phenazine **6** also sits within the cavity of the macrocycle by a combination of hydrogen bonds (dNH$\cdots$N$_{phen}$= 2.17 Å, dNH$\cdots$O$_{phen}$= 2.07 Å and 2.15 Å) and π-stacking at distances of 3.42 and 3.50 Å to the external anthracenes. Furthermore, the pseudorotaxane **6@1** piles up in 1D columns with a distance of 3.60 Å between anthracenes.

In the crystal structure of pseudorotaxane **7@1** (triclinic *P-1*), the macrocycle adopts a boat like conformation (Figure 3) with two different angles (169^{o} and 130^{o}), in a structure similar to the analogous pseudorotaxane **4@1**. Four hydrogen bond distances are observed between the amides and the oxygen atoms of phenazine **7** (dNH$\cdots$O$_{phen}$ = 2.08, 2.13, 2.19 and 2.23 Å) and four intramolecular hydrogen bonds with the pyridinic ring of the macrocycle (dNH$\cdots$N$_{pyr}$ = 2.43, 2.38, 2.48 and 2.39 Å). Again the phenazine **7** is π-stacked to the external anthracenes at distances of 3.40 and 3.44 Å. Pseudorotaxane **7@1** also piles up in 1D columns with interplanar distances between anthracenes of 3.61 Å.

5. Theoretical calculations

All calculations were performed with Gaussian09 with the exception of the resonant Raman that was performed with Gaussian16.[4,5] Properties on two different geometries were computed, with molecular, i.e. non-periodic, models:

1) **crystalline geometries**, where the molecular initial positions for a complex were *cut* from the CIF files obtained by fitting XRD data, followed by a partial optimization, where the heavy atoms (C, N and O) were fixed and only H atoms were optimized at the B3LYP/6-31+g(d,p) with the D3BJ correction of Grimme.[6,7] This procedure was used for most crystalline structures, namely for 2@1, 3@1, 4@1, 5@1, and 7@1 as no further optimization was needed. For, 6@1, the molecular geometry was not accurate enough for a single point quantum calculation and had to be further refined. For this, an extra optimization procedure, where the phenazine and anthracenes were partially optimized for a low number optimization cycles were additionally performed yielding the 6@1* structure. These crystalline geometries were used for computing the electronic properties in this study, namely: HOMO-LUMO gaps, eigenvalues and electronic spectra.
2) **molecular geometries** were obtained by full optimization in solution. Molecular geometries were used for computing the vibrational frequencies and the Raman and resonant Raman spectra.

Table S3. Molecular orbital eigenvalues at the B3LYP/6-31+g(d,p) level for the crystalline geometries. For 6@1*, the molecular geometry of phenazines and anthracenes are partially optimized (see above). All energies are in eV.

	LUMO+2	LUMO+1	LUMO	HOMO	HOMO-1	HOMO-2	gap
2@1	-2.37	-2.37	-3.22	-5.72	-5.82	-6.71	**2.5**
1 (2@1)	-1.98	-2.46	-2.46	**-5.89**	-5.9	-7.14	3.43
2	-0.48	-0.96	**-2.77**	-6.38	-7.06	-7.21	3.61
3@1	-2.31	-2.38	-3.46	-5.74	-5.83	-6.53	**2.28**
1 (3@1)	-1.99	-2.39	-2.4	**-5.86**	-5.87	-7.05	3.46
3	-0.7	-1.16	**-2.99**	-6.04	-7.48	-7.59	3.05
4@1	-2.31	-2.35	-3.67	-5.78	-5.84	-6.36	**2.11**
1 (4@1)	-2.01	-2.31	-2.32	**-5.8**	-5.83	-6.97	3.48
4	-0.92	-1.57	**-3.26**	-5.73	-7.44	-7.46	2.47
5@1	-2.09	-2.17	-2.95	-5.51	-5.63	-6.18	**2.56**
1 (5@1)	-2.03	-2.28	-2.29	**-5.74**	-5.74	-6.96	**3.45**
5	-0.17	-0.72	**-2.38**	-5.89	-6.65	-6.76	3.51
6@1*	-2.29	-2.39	-3.3	-5.63	-5.78	-6.34	**2.33**
1 (6@1)*	-2.11	-2.42	-2.49	**-5.82**	-5.88	-7.01	3.33
6*	-0.47	-0.93	**-2.7**	-5.79	-6.66	-7.16	3.09
7@1	-2.22	-2.27	-3.39	-5.6	-5.7	-6.07	**2.21**
1 (7@1)	-2.03	-2.3	-2.31	**-5.71**	-5.76	-6.94	3.4
7	-0.66	-1.21	**-2.95**	-5.44	-6.82	-7.2	2.49

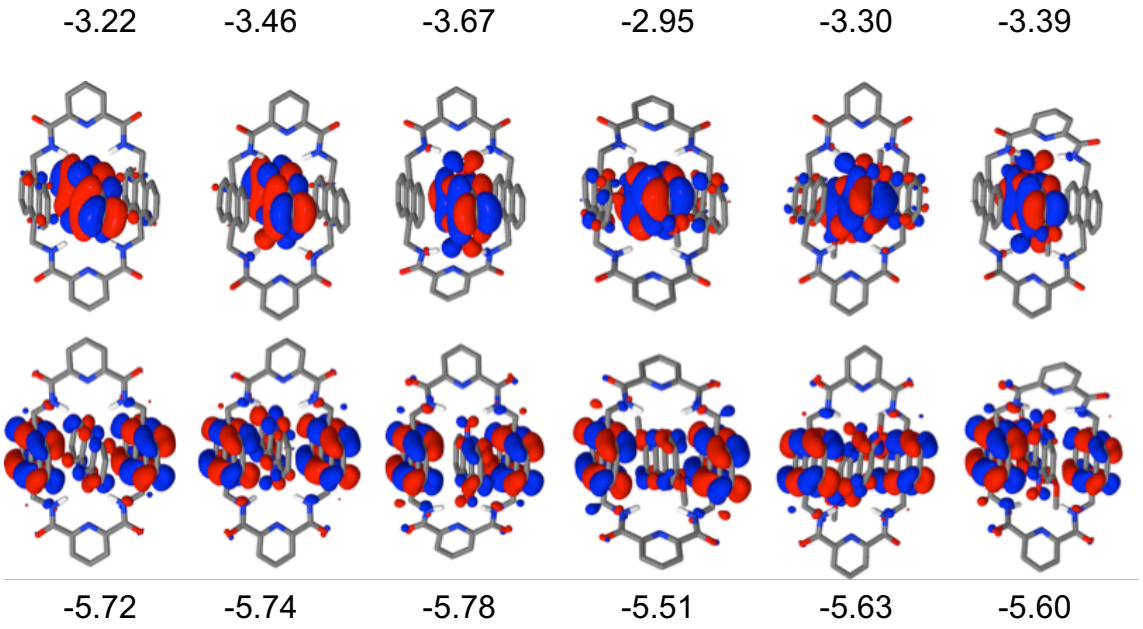

Figure S5. HOMO (bottom) and LUMO (top) of **2@1**, **3@1**, **4@1**, **5@1**, **6@1** and **7@1** (from left to right) at the M06-2X/6-31+g(d,p) level and corresponding energies with B3LYP (eV).

6. Raman Spectroscopy

The 1064 nm FT–Raman spectra were obtained with an FT–Raman accessory kit (FRA/106–S) of a Bruker Equinox 55 FT-IR interferometer. A continuous–wave Nd-YAG laser working at 1064 nm was employed for excitation. A germanium detector operating at liquid nitrogen temperature was used. Raman scattering radiation was collected in a back–scattering configuration with a standard spectral resolution of 4 cm^{-1}. 1000–3000 scans were averaged for each spectrum. The spectrum recorded at 532 nm were collected by using a Invia Qontor Raman Confocal Microscope (RENISHAW) with a spectral resolution of ±1 cm^{-1}. The detector used was a CCD Camera Renishaw Centrus electrically cooled by a peltier. A laser power of 0,27 mW was used with 5 scans of 10 seconds of acquisition time, 50x magnification. a spectral range of 100-3200 cm^{-1}.

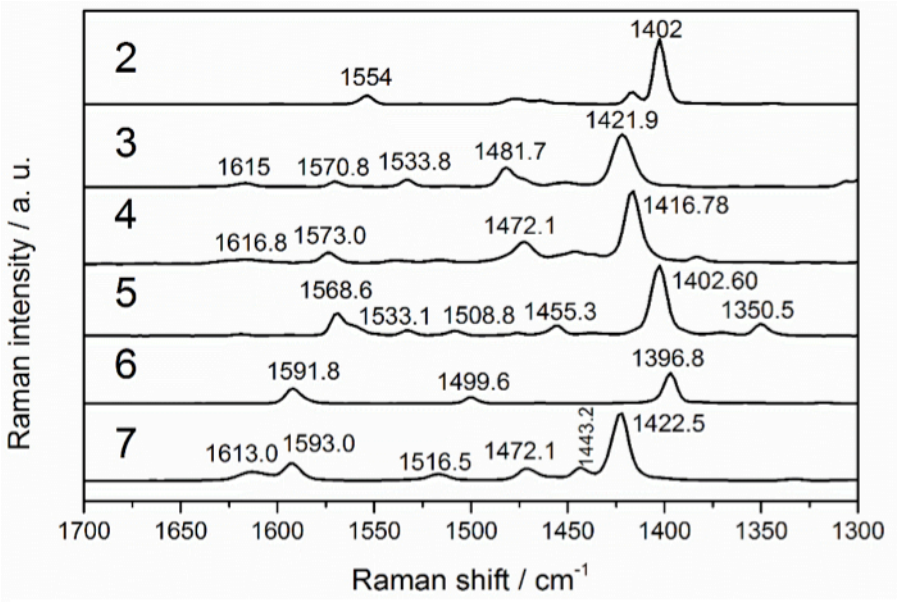

Figure S6: Solid state FT-Raman spectra recorded with the 1064 nm excitation wavelength for the individual phenazines **2**-**7**.

The Amide I stretching modes of the amides of macrocycle **1** mainly involve the stretching vibration of their carbonyls [i.e., ν (C=O)] and, as a result, are weak Raman bands around 1670-1650 cm^{-1} is observed. Interestingly, a comparison of the Amide I frequency of **1** (1672.2 cm^{-1}) with those of the pseudorotaxanes (Figure 6) evidence changes in the frequency of the Amide I frequency band. This hint in the vibrational spectra is revealing a two-fold mode of coupling between the two chromophores, either by π-π overlap, with or without charge polarization (with an associated photoinduced charge transfer in the absorption spectrum), or by forming H bonds between the nitrogens of the phenazine and the hydrogens of the amides of **1**. When these are formed, the resonance of the nitrogen lone electron pair over the carbonyl group carbonyl increases by which the contribution of the enolate form (O=C–N(R)–H → $^{-}$O–C=N(R)$^{+}$–H••••N) increases and the ν (C=O) frequency decreases.

7. Time-Resolved Microwave Conductivity

Laser-flash TRMC experiments were conducted for the sample on a quartz plate using the third harmonic generator (THG; 355 nm) of a Nd:YAG laser (Continuum Inc., Surelite II, 5–8 ns pulse duration, 10 Hz) as the excitation source (9.1 × 10^{15} photons cm^{-2} $pulse^{-1}$). The frequency and power of microwave were ~9.1 GHz and 3 mW, respectively. The photoconductivity transient Δσ was converted to the product of the quantum yield (φ) and the sum of charge carrier mobilities $\sum\mu$ (= μ_+ + μ_-) by the formula $\varphi\sum\mu = \Delta\sigma(eI_0F_{light})^{-1}$, where e and F_{light} are the unit charge of a single electron and a correction (or filling) factor, respectively.

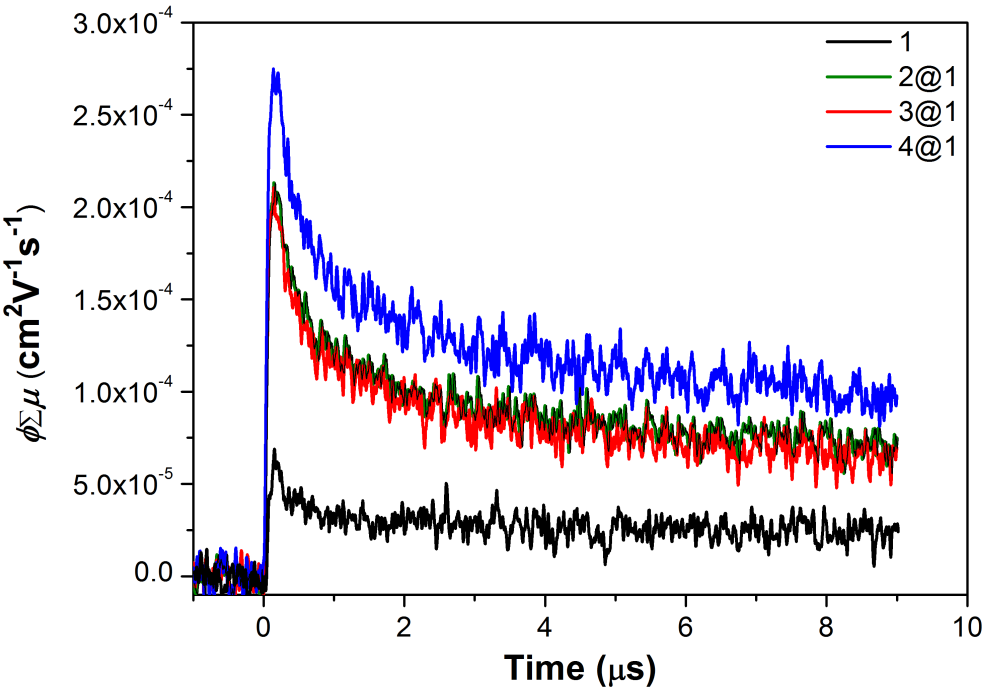

Figure S7. Pseudo-Photocurrent transients observed for macrocycle **1** and pseudorotaxanes **2@1**-**4@1**.

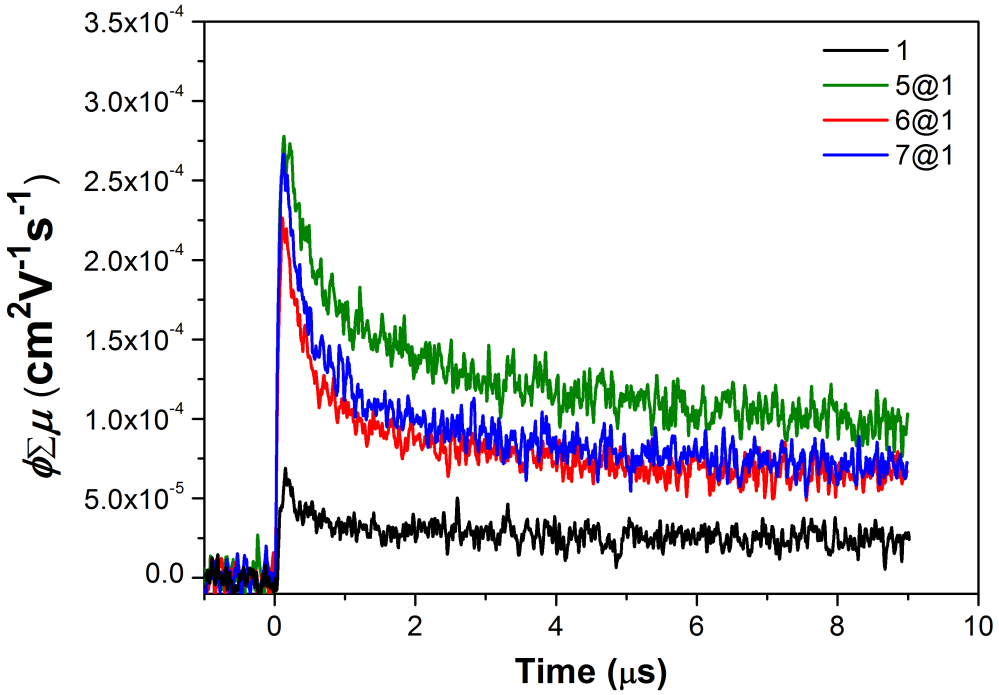

Figure S8. Pseudo-Photocurrent transients observed for macrocycle **1** and pseudorotaxanes **5@1**-**7@1**.

8. Bibliography

1. J. J. Gassensmith, E. Arunkumar, L. Barr, J. M. Baumes, K. M. DiVittorio, J. R. Johnson, B. C. Noll, and B. D. Smith *J. Am. Chem. Soc.* 2007*,* **129,** 15054–15059.
2. Y. Kobayashi, I. Kumadaki, H. Sato, Y. Sekine, and T. Hara, *Chem. Pharm. Bull. (Tokyo).* 1974, **22**, 2097–2100.
3. I. Yosioka and H. Otomasu *Pharm. Bull.* 1953, **1**, 66–69.
4. Gaussian 09, Revision A.02, M. J. Frisch, G. W. Trucks, H. B. Schlegel, G. E. Scuseria, M. A. Robb, J. R. Cheeseman, G. Scalmani, V. Barone, G. A. Petersson, H. Nakatsuji, X. Li, M. Caricato, A. Marenich, J. Bloino, B. G. Janesko, R. Gomperts, B. Mennucci, H. P. Hratchian, J. V. Ortiz, A. F. Izmaylov, J. L. Sonnenberg, D. Williams-Young, F. Ding, F. Lipparini, F. Egidi, J. Goings, B. Peng, A. Petrone, T. Henderson, D. Ranasinghe, V. G. Zakrzewski, J. Gao, N. Rega, G. Zheng, W. Liang, M. Hada, M. Ehara, K. Toyota, R. Fukuda, J. Hasegawa, M. Ishida, T. Nakajima, Y. Honda, O. Kitao, H. Nakai, T. Vreven, K. Throssell, J. A. Montgomery, Jr., J. E. Peralta, F. Ogliaro, M. Bearpark, J. J. Heyd, E. Brothers, K. N. Kudin, V. N. Staroverov, T. Keith, R. Kobayashi, J. Normand, K. Raghavachari, A. Rendell, J. C. Burant, S. S. Iyengar, J. Tomasi, M. Cossi, J. M. Millam, M. Klene, C. Adamo, R. Cammi, J. W. Ochterski, R. L. Martin, K. Morokuma, O. Farkas, J. B. Foresman, and D. J. Fox, Gaussian, Inc., Wallingford CT, 2016.
5. Gaussian 16, Revision A.03, Frisch, M. J.; Trucks, G. W.; Schlegel, H. B.; Scuseria, G. E.; Robb, M. A.; Cheeseman, J. R.; Scalmani, G.; Barone, V.; Petersson, G. A.; Nakatsuji, H.; Li, X.; Caricato, M.; Marenich, A. V.; Bloino, J.; Janesko, B. G.; Gomperts, R.; Mennucci, B.; Hratchian, H. P.; Ortiz, J. V.; Izmaylov, A. F.; Sonnenberg, J. L.; Williams-Young, D.; Ding, F.; Lipparini, F.; Egidi, F.; Goings, J.; Peng, B.; Petrone, A.; Henderson, T.; Ranasinghe, D.; Zakrzewski, V. G.; Gao, J.; Rega, N.; Zheng, G.; Liang, W.; Hada, M.; Ehara, M.; Toyota, K.; Fukuda, R.; Hasegawa, J.; Ishida, M.; Nakajima, T.; Honda, Y.; Kitao, O.; Nakai, H.; Vreven, T.; Throssell, K.; Montgomery, J. A., Jr.; Peralta, J. E.; Ogliaro, F.; Bearpark, M. J.; Heyd, J. J.; Brothers, E. N.; Kudin, K. N.; Staroverov, V. N.; Keith, T. A.; Kobayashi, R.; Normand, J.; Raghavachari, K.; Rendell, A. P.;

Burant, J. C.; Iyengar, S. S.; Tomasi, J.; Cossi, M.; Millam, J. M.; Klene, M.; Adamo, C.; Cammi, R.; Ochterski, J. W.; Martin, R. L.; Morokuma, K.; Farkas, O.; Foresman, J. B.; Fox, D. J. Gaussian, Inc., Wallingford CT, 2016.

6. S. Grimme, J. Antony, S. Ehrlich and H. A. Krieg *J. Chem. Phys.* 2010 **132**., 154104.
7. S. Grimme, S. Ehrlich and L. Goerigk, *J. Comput. Chem.* 2011, **32,** 1456–1465.